Linearized rate-equation approach for double-well systems:
Cooling- and temperature-dependent low-field magnetization of magnetic nanoparticles

Paolo Allia,[1,2,*] Gabriele Barrera,[2] and Paola Tiberto[2]

[1]*DISAT, Politecnico di Torino, Corso Duca degli Abruzzi 24, I-10129 Torino, Italy*
[2]*INRIM, Nanoscience and Materials, strada delle Cacce 91, 10135 Torino (TO), Italy*

Low-field magnetization curves for an assembly of polydisperse magnetic nanoparticles described as double-well systems (DWS) with randomly distributed easy axes are generated by means of a rate-equation approach applied to states obtained by cooling with and without a magnetic field. The model has notable advantages over the existing steady-state approaches, allowing one to accurately determine the magnetization frozen in a sample after cooling under field, and to study the effect of the magnitude of the cooling field on the shape of the field-cooled (FC) curve. The DWS scheme keeps validity well above the blocking temperature, making it possible to apply the model over all the region of interest (i.e., when the system is out of equilibrium). A linearized expression for the magnetization curves is obtained and compared with the existing formulas. It is shown that the linearized expression for the zero-field-cooled (ZFC) curve is more satisfactory, while no linearized expression for the FC curve is able to accurately reproduce the behavior derived from the rate equations. A method to obtain the size distribution function is developed; this makes use of the linearized model in the DWS scheme and is based on the analysis of the experimental ZFC curve only. Explicit expressions for the FC/ZFC curves of DWS characterized by an average blocking temperature higher than the starting temperature of the measurement cycle are proposed and shown to naturally explain "anomalous" experimental curves found in the literature.

I. INTRODUCTION

Magnetic nanoparticles have become one of the most studied topics of present-day magnetism; the rise of research activity has been boosted by their many potential applications in a variety of areas ranging from ICTs to magnetic recording, environmental protection, biomedicine, biotechnology [1–8]; from the standpoint of basic science, they still represent a unique test ground to validate simple ideas. The properties of magnetic nanoparticles are studied through a wide variety of approaches and techniques, among which a central role is played by DC and AC magnetization measurements. Among DC measurements, zero-field-cooled and field-cooled (ZFC/FC) magnetization curves have become an outstanding method of analysis; their presence in experimental papers is nowadays ubiquitous and the existing literature is vast [9–11]. As a matter of fact, FC/ZFC curves provide interesting information about a nanoparticle system: In principle, their analysis gives an estimate of the average magnetic moment of nanoparticles [12], the distribution of nanoparticle sizes [13,14], the dominant anisotropy energy [15,16], and the presence of interactions [17,18] responsible for ordered or disordered states at low temperatures [19]. However, the advancement of knowledge is somewhat hindered by the circumstance that FC/ZFC curves are typically analyzed on the basis of qualitative rather than quantitative grounds. Sensible arguments and simple methods to extract physical properties from FC/ZFC curve fits have been proposed in

the past [13,14,20] and are generally followed, albeit sometimes uncritically, by the scientific community. Typically, these methods make use of simplifying assumptions: (a) each nanoparticle coherently behaves as a macrospin [9]; (b) the nanoparticles are noninteracting; (c) the effective magnetic anisotropy energy (which may take into account weak interparticle interactions [21–23]) has uniaxial symmetry; (d) the kinetics of macrospin redistribution between the minima of energy obeys the classical Arrhenius law; (e) in thermal equilibrium, the nanoparticles are in the ideal superparamagnetic regime described by the Langevin function; (f) the field applied during FC/ZFC curve measurements is so small that the response of the nanoparticle's magnetic moment is linear; (g) the transition from blocked to superparamagnetic behavior is very sharp and occurs exactly at the particle's blocking temperature T_B. Although the Arrhenius kinetic law naturally involves the *time* variable, the simplified models for FC/ZFC curves available in the literature strictly refer to the steady state of the system, so that time is never explicitly taken into account; in the end this produces a defect of knowledge. As a matter of fact, rate equations were employed by Usov [24] to describe FC/ZFC curves of polydisperse uniaxial nanoparticles. Similarly, rate equations were exploited to study some effects in the particular case of monodisperse particles submitted to a magnetic field parallel to the easy anisotropy axis [25–28]. The common limitation of these methods is the intrinsic difficulty of transforming rigorous numerical results into a simplified model; as a consequence, it becomes impossible to compare rate-equation results with the available steady-state models in order to clarify the limits of validity of the latter.

*Corresponding author: paolo.allia@polito.it

The aim of this paper is to fill this gap by approaching the problem from the rate-equations standpoint and then developing a simplified form. In order to compare the results of the present model with the existing literature, assumptions (a) to (d) of the above list are maintained. The uniaxial anisotropy allows one to describe each nanoparticle as a classical double-well system (DWS); the macrospin can switch between energy minima obeying the rate equations whose time constants are determined at each temperature by the Arrhenius law. Describing a single nanoparticle as a DWS is the customary framework when the blocked state of a nanoparticle system is investigated [29]. However, the existing models [13,14,20] for FC/ZFC curve analysis assume that immediately above T_B the nanoparticle enters the ideal superparamagnetic state, which is not a DWS state. In fact, it has long since been shown by Fruchart *et al.* [30,31] that ideal superparamagnetism (intended as one whose equilibrium magnetization is described by the Langevin law) can be viewed as a high-temperature limit of the magnetic response of a DWS. Their model, based on standard thermal physics methods, provides an exact expression for the equilibrium magnetization when the easy axis of the DWS is parallel to the applied field direction. For a generic angle between these axes, a numerical solution can be easily set up. Although originally derived for a slightly different physical system, the approach by Fruchart *et al.* can be extended to uniaxial nanoparticles as well [31], indicating that a representation as DWS is appropriate until the temperature becomes so high that $k_B T \gg K_{eff} V$, K_{eff} being the effective anisotropy constant and V the nanoparticle volume. This implies that the DWS picture can be applied well above the average blocking temperature, at least up to $5T_B$, and that it slowly transforms into the standard superparamagnetic picture (magnetization proportional by the Langevin law) at even higher temperatures. Therefore, the rate equation method is safely applicable below and above T_B with the proviso that the maximum investigated temperature T_{MAX} be roughly of the order of $5T_B$, i.e., well above the region where all notable properties of the FC/ZFC appear.

The rate-equation approach is then transformed to provide much simpler, analytically manageable formulas which can be directly compared to the steady-state expressions circulating in the literature. As we shall see, this will prove that the existing linearized methods of analysis can lead to incorrect conclusions, providing, e.g., a wrong estimate of the average magnetic moment or the effective anisotropy of a system of nanoparticles. In addition, it will be shown that the formulas for FC curves available in the literature are affected by a systematic error.

The linearized expressions of the ZFC curve in the DWS scheme allow one to get a more reliable estimate of the size distribution function $p(D)$ of a polydisperse nanoparticle system. A method to derive the $p(D)$ curve making use of the linearized ZFC curve alone will be described in detail.

Finally, analysis of the rate equations and of their linearization will show that the existing steady-state models fail to represent the FC/ZFC magnetization when the average blocking temperature is well above T_{MAX}, allowing many "anomalous" experimental curves found in the literature to be naturally explained.
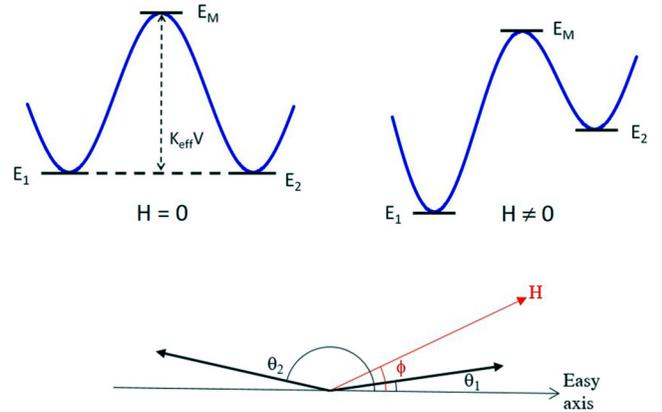
FIG. 1. Parameters of the rate-equation model for a DWS. Top sketch: DWS energy landscape without and with applied field; bottom image: reference system for the DWS (easy axis parallel to the x axis).

II. RATE EQUATIONS

Each magnetic nanoparticle is assumed to be characterized by a size D and an effective volume $V = (\pi/6)D^3$. Nanoparticles are distributed in size according to a continuous distribution law $p(D)$. Each nanoparticle of size D carries a magnetic moment $\mu = M_s V$ where M_s is the saturation magnetization of the material; in the absence of a magnetic field the magnetic moment is aligned by uniaxial anisotropy to an easy axis, and the two equivalent energy minima are separated by the anisotropy barrier $K_{eff} V$. The average blocking temperature $\langle T_B \rangle$ is defined as $K_{eff}\langle V\rangle/25k_B$, $\langle V \rangle$ being the average volume. In general, both M_s and K_{eff} are functions of temperature. All model's parameters are reported in Fig. 1, where the x-y plane is defined by the applied field H and the easy axis of each nanoparticle, described as a double-well system (DWS).

Although the easy axis directions of all nanoparticles in the material are evenly distributed in 3D space, a simple planar representation of the single DWS is perfectly adequate to describe the investigated effects: In each nanoparticle, the easy axis and the field axis univocally define a plane; symmetry implies that the switching of magnetization between the two minima occurs in this plane; in systems of randomly oriented nanoparticles the angle ϕ is evenly distributed between 0 and 2π, however, for symmetry reasons, it is sufficient to consider ϕ between $-\pi/2$ and $+\pi/2$. A completely different case would arise in nanoparticles characterized by anisotropies of higher symmetry (such as, e.g., cubic anisotropy): There, magnetization switching between local minima of energy would imply complex trajectories of the magnetization vector in three dimensions; these trajectories would in turn depend on both direction and magnitude of the applied field. Let us consider a number N_ϕ of particles of given magnetic moment μ with easy axis at an angle ϕ with respect to H. For evenly distributed easy-axis directions, $N_\phi = N/\pi$, N being the total number of particles of volume V. The magnetization of this subset along the direction of the field is

$$M(T, \phi) = N_1(T)\mu\cos(\theta_1(T) - \phi)$$
$$+ N_2(T)\mu\cos(\theta_2(T) - \phi). \quad (1)$$

The equilibrium values of N_1 and N_2 at the temperature T [32] can be put in the form:

$$N_1(T) = \frac{N_\phi}{1 + e^{-\alpha}}$$

$$N_2(T) = \frac{N_\phi e^{-\alpha}}{1 + e^{-\alpha}}, \tag{2}$$

where $\alpha = \frac{E_2 - E_1}{k_B T}$, $E_i = E(\theta_i, T)$ is the two energy minima in the double well, i.e.:

$$E(\theta_{1,2}, T) = K_{\text{eff}} V \sin^2\theta_{1,2}(T) - M_S H V \cos(\theta_{1,2}(T) - \phi). \tag{3}$$

The angles of minimum energy $\theta_1(T)$, $\theta_2(T)$ are found as usual by putting the derivative of $E(\theta, T)$ equal to zero for any temperature. Taking into account that $N_2 = N_\phi - N_1$, Eq. (1) transforms into

$$M(T, \phi) = M_1(T)(\cos(\theta_1(T) - \phi) - \cos(\theta_2(T) - \phi)) + M_{s\phi}\cos(\theta_2(T) - \phi), \tag{4}$$

where $M_1 = N_1\mu$, $M_{s\phi} = N_\phi\mu$; $M_{s\phi} = M_s/\pi$.

The rate equations for this set of DWS are:

$$\frac{dN_1}{dt} = -\frac{N_1}{\tau_1} + \frac{N_2}{\tau_2}$$

$$\frac{dN_2}{dt} = \frac{N_1}{\tau_1} - \frac{N_2}{\tau_2}. \tag{5}$$

In the Arrhenius approach $\tau_i = \tau_0 e^{\frac{E_M - E_i}{k_B T}}$, $\tau_0(\approx 10^{-9}s)$ being the usual pre-exponential factor (see Fig. 1) [33]. For simplicity's sake, in the following it will be assumed $ln(\tau_0/\tau_{\text{meas}}) = 25$, τ_{meas} being the typical measurement time ($=100$ s according to the literature [14]). It should be noted that in the Arrhenius approach relaxation times τ_1 and τ_2 are predicted without making reference to the details of the actual dynamics of magnetization reversal, as depicted by more in-depth analysis based on the Landau-Lifshitz (LL) or Landau-Lifshitz-Gilbert (LLG) equations. However, relaxation times for Arrhenius-type barrier crossing are typically higher than the ones obtained in the LL/LLG approach (which are of the order of 10–500 ps for damping factors of the order of 0.01–0.2 [34,35]), meaning that the rate-determining process is thermally activated barrier crossing.

In steady state, $dN_1/dt = dN_2/dt = 0$ and the equilibrium magnetization is recovered. Exploiting $N_2 = N_\phi - N_1$, Eqs. (5) can be rewritten in terms of a single equation for $M_1(T, t)$:

$$\frac{dM_1}{dt} = -\frac{\tau_1 + \tau_2}{\tau_1\tau_2}M_1 + \frac{M_{s\phi}}{\tau_2}, \tag{6}$$

where $\tau_{1,2} = \tau_{1,2}(t)$ because temperature $T = T(t)$ is time dependent. Such an equation is easily solved numerically for $M_1(T, t)$ by writing

$$\Delta M_1 = \left[-\frac{\tau_1 + \tau_2}{\tau_1\tau_2}M_1 + \frac{M_{s\phi}}{\tau_2} \right]\Delta t \tag{7}$$

and taking sufficient small Δt intervals in order to ensure that at each step of the forward Euler method adopted to solve Eq. (7) the condition $|\Delta M_1| \leqslant 0.01 M_1$ is satisfied from T_{min}

up to $1.4 \times T_B$, i.e., well inside the fully reversible region. Further details are given in the Supplemental Material (Sec. 1) [36]; in this work, Δt was taken equal to 1×10^{-4} s. The relationship between temperature and time is assumed to be linear: $T(t) = T_{\text{min/MAX}} \pm \beta_{h/c}t$, where $\beta_{h/c}$ are the heating/cooling rates which are typically different from each other. The solutions of Eq. (7) depend to some extent on the heating/cooling rates $\beta_{h/c}$. The single parameter $M_1(T)$ plays a central role in the model: Once Eq. (7) is integrated, the magnetization in the direction of the field is immediately given by Eq. (4).

A. Initial/final values of $M_1(T)$

We suppose that the temperature interval of interest spans between a minimum $T_{\text{min}}(\approx 0K)$ and a maximum T_{MAX}. The initial values of the quantity M_1 differ for ZFC and FC curves.

In the ideal ZFC condition, the N_ϕ nanoparticles are evenly distributed in either well, so that $M_1(T_{\text{min}}) = M_{s\phi}/2$; all $M_1(T)$ values including $M_1(T_{\text{MAX}})$ result from direct integration of Eq. (7). The corresponding extremal values of $M(T, \phi)$ are obtained evaluating Eq. (4) at $T = T_{\text{min}}$ and T_{MAX}. Note that when $T_{\text{MAX}} \gg \langle T_B \rangle$, $M_1(T_{\text{MAX}})$ becomes equal to $M_{s\phi}/(1 + e^{-\alpha(T_{\text{MAX}})})$ and the magnetization reaches the equilibrium value; else, $M_1(T_{\text{MAX}})$ is still far from equilibrium (typically, well below the equilibrium curve at T_{MAX}; see Sec. V). Examples of $M(T, \phi)$ curves obtained from the solution of Eq. (7) for a given nanoparticle size and different values of ϕ are shown in Fig. 2 along with the corresponding equilibrium curves; the average over all ϕ values $M(T)$ is also reported. According to the assumption of randomly distributed easy axes, a simple arithmetic mean over N angles
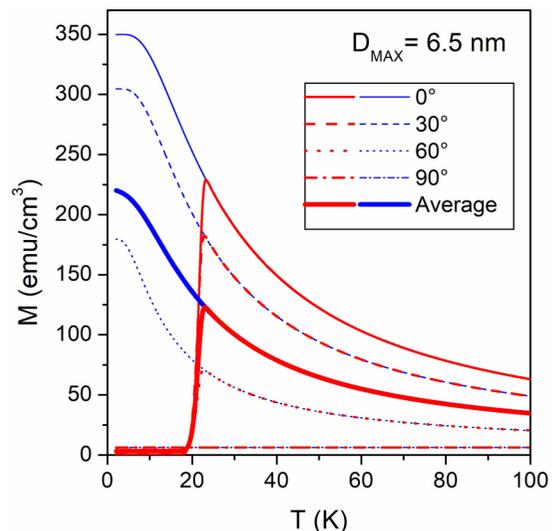
FIG. 2. Red lines: Temperature dependence of the ZFC magnetization obtained solving the rate equations for monodisperse nanoparticles of size $D = 6.5 \times 10^{-7}$ cm with easy axes making different angles ϕ with the magnetic-field direction; thick line: average over all ϕ angles evenly distributed between $-\pi/2$ and $\pi/2$. Blue lines: corresponding equilibrium curves; thick line: average over all ϕ angles. Saturation magnetization $M_s = 350$ emu/cm^3; effective anisotropy constant $K_{\text{eff}} = 5 \times 10^5$ erg/cm^3, measurement field $H = 50$ Oe, heating rate $\beta_h = 6$ K/min.

between $\phi = -\pi/2$ and $\phi = \pi/2$ was performed, with $N = 181$. It was checked that the relative difference between this average and the one done with $N = 1801$ was negligible ($<2 \times 10^{-3}$).

As is well known, the FC curve is measured after cooling down the sample from T_{MAX} to T_{min} under a cooling field H_f. The effect is to freeze a starting value of magnetization substantially different from the previous case. In the standard experimental practice [37] the magnetization is not recorded on cooling and is measured in the subsequent heating only; typically, the experimental protocol asks for the same field H to be applied on cooling and heating ($H_f = H$), however, in general the cooling field H_f may differ from the measurement field H and can give rise to different starting values for the FC curve. The rate-equation model allows one to follow the freezing process from T_{MAX} to T_{min} under arbitrary H_f and to find the exact value of the frozen-in magnetization at T_{min}.

In the freezing process, one starts from the value of M_1 at T_{MAX} as obtained after completion of the ZFC curve; the value of M_1 at T_{min} is found by integrating Eq. (7) and is markedly dependent on H_f. The corresponding frozen-in magnetization value is called M_f^*:

$$M_f^* = M_1(T_{min})(\cos(\theta_{1f}(T_{min}) - \phi) - \cos(\theta_{2f}(T_{min}) - \phi))$$
$$- M_{s\phi}\cos(\theta_{2f}(T_{min}) - \phi), \quad (8)$$

where θ_{1f} and θ_{2f} are the angles of tilt of the magnetization away from the directions $\theta = 0$, π by effect of the field H_f.

It should be explicitly noted that the value of M_f^* is determined by two concurring effects:

(1) The main contribution to M_f^* arises from the uneven distribution of DWS in the two wells because of the effect of field H_f on cooling; such a term can be named as "intrinsic" and indicated by M_{intr}^*.

(2) A second contribution arises from the tilt angles θ_{1f} and θ_{2f} towards the field direction; this acts to further slightly increase the frozen-in magnetization above the intrinsic value and is linearly dependent on the magnitude of H_f. The two quantities are related by (see Appendix A 1):

$$M_f^* = M_{intr}^* + M_{s\phi}\frac{M_s H_f}{2K_{eff}}\sin^2\phi. \quad (9)$$

If the freezing field is removed after cooling, the frozen-in magnetization is M_{intr}^* which has the following simple expression, obtained putting $\theta_{1f} = 0$ and $\theta_{2f} = \pi$ in Eq. (8):

$$M_{intr}^* = [2M_1(T_{min}) - M_{s\phi}]\cos\phi. \quad (10)$$

Examples of cooling curves and of the resulting quantities M_f^* and M_{intr}^* are shown in Fig. 3 for different values of the freezing field H_f. The magnetization freezes over a finite temperature interval around T_B. Of course, the frozen-in magnetization weakly depends on the cooling rate β_c also; an example is reported in the Supplemental Material [36] (Sec. 2).

Although M_{intr}^* is the frozen-in magnetization ascribed to the redistribution of DWS in the two wells only, usually this is the only term taken into account by the available simplified models of FC curves [14,20]. However, the real frozen-in magnetization (M_{intr}^*) is systematically larger; the difference is non-negligible, particularly when H_f is above 20 Oe (as
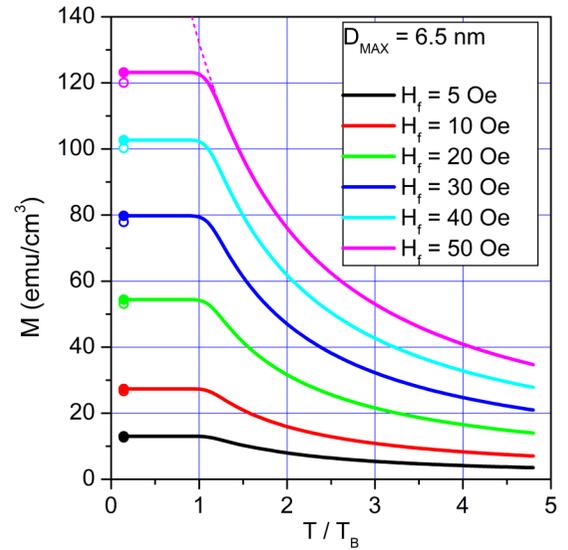
FIG. 3. Cooling curves for monodisperse nanoparticles (parameter values as in Fig. 2, cooling rate $\beta_c = 50$ K/min) obtained solving the rate equations for different values of the cooling field H_f, after averaging over all ϕ angles. The reduced temperature T/T_B is used. Dashed line: equilibrium magnetization curve for $H = 50$ Oe. The frozen-in magnetizations M_f^* and $Mintr^*$ are shown as full and open dots, respectively.

it usually happens in actual measurements). It should be explicitly remarked that not only the magnitude but also the shape of the freezing curves depends on H_f.

When the system is subsequently heated to T_{MAX}, the quantity M_1 is again obtained by integrating Eq. (7) starting from the initial value $M_1(T_{min})$; the initial value of the FC magnetization is

$$M^* = M_1(T_{min})[\cos(\theta_1(T_{min}) - \phi) - \cos(\theta_2(T_{min}) - \phi)]$$
$$+ M_{s\phi}\cos(\theta_2(T_{min}) - \phi). \quad (11)$$

This value differs from M_f^* if $H \neq H_f$, because in that case $\theta_1 \neq \theta_{1f}$, $\theta_2 \neq \theta_{2f}$.

The steps described so far make explicit reference to a specific angle ϕ and a fixed value of D. The curves corresponding to summation over all angles and all nanoparticle sizes—described by the $p(D)$ distribution function—are henceforth obtained in a straightforward way.

Some examples of FC/ZFC curves obtained solving the rate equations for different nanoparticle distributions are given in Fig. 4. The $p(D)$ curves are assumed to be lognormal functions with different values of the median D_{MAX} and of σ. For simplicity, K_{eff} and M_s were considered to be constant ($K_{eff} = 5 \times 10^5$ erg/cm^3, $M_s = 350$ emu/cm^3).

It is possible to check that using a monotonically decreasing $M_s(T)$ law compatible with actual measurements on real nanoparticle systems, and a power law of type $K_{eff}(T) \sim M_s(T)^n$ ($n = 2$–10) for the effective anisotropy, the shape of both FC/ZFC curves is just slightly modified with respect to the case of constant M_s and K_{eff} discussed here; the changes are so small that they only marginally affect the interpretation of the curves. For this reason, the case of variable M_s and K_{eff} will not be further treated in this paper.
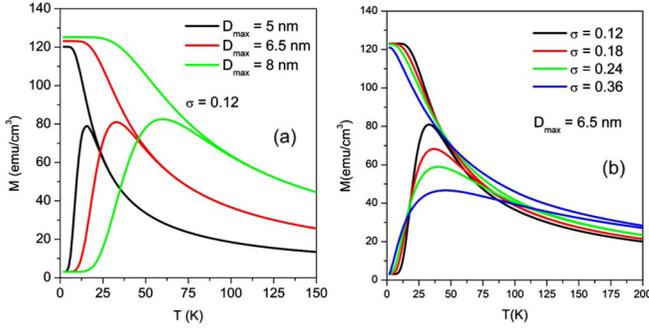
FIG. 4. Temperature dependence of the FC/ZFC curves obtained solving the rate equations for nanoparticles distributed in size according to a lognormal distribution (heating rate $\beta_h = 6$ K/min, cooling rate $\beta_c = 50$ K/min). Panel (a): different median values of $D(D_{\max})$ and same σ. Panel (b) different σ values and same $D_{\max}$. Parameter values as in Fig. 2.

III. LINEARIZATION OF THE DWS RATE-EQUATION MODEL

All existing approaches to the analysis of experimental FC/ZFC magnetization curves have the notable advantage of providing simple, handy expressions which allow one to fit experimental curves with the aim of getting information about physical quantities such as the effective anisotropy or the particle size distribution $p(D)$ [13,14,20].

The expressions for M_{ZFC} and M_{FC} currently exploited in the literature can be recast in the following form:

$$M_{ZFC}(T) = \frac{M_s^2 H}{3k_B T} \int_0^{D_c(T)} V p(D) dD$$

$$+ \frac{M_s^2 H}{3K_{\text{eff}}} \int_{D_c(T)}^{\infty} p(D) dD$$

$$M_{FC}(T) \simeq \frac{M_s^2 H}{3k_B T} \int_0^{D_c(T)} V p(D) dD$$

$$+ \frac{25 M_s^2 H}{3K_{\text{eff}}} \int_{D_c(T)}^{\infty} p(D) dD$$

$$= M_{ZFC}(T) + \frac{8 M_s^2 H}{K_{\text{eff}}} \int_{D_c(T)}^{\infty} p(D) dD, \quad (12)$$

where $D_c(T) = \frac{6}{\pi} (25 k_B T / K_{\text{eff}})^{\frac{1}{3}}$; in both lines, the first integral refers to the smaller nanoparticles which are in the superparamagnetic regime at the temperature T and the second integral to larger nanoparticles which are still in the blocked state. It should be noted that both expressions are based upon two main simplifying assumptions:

(a) For each D, the transition between the blocked and the superparamagnetic behavior at T_B is extremely sharp. This brings about discontinuities in both ZFC and FC curves at T_B (in the first case, a discontinuity of M; in the second case, a discontinuity of its derivative dM/dH). These discontinuities disappear upon averaging over parameter D. In fact, rate equations indicate that the blocked-to-superparamagnetic transition is not so sharp, so that the equilibrium curve is attained over a finite, non-negligible temperature region around T_B; an example of the difference between the prediction of Eq. (12)
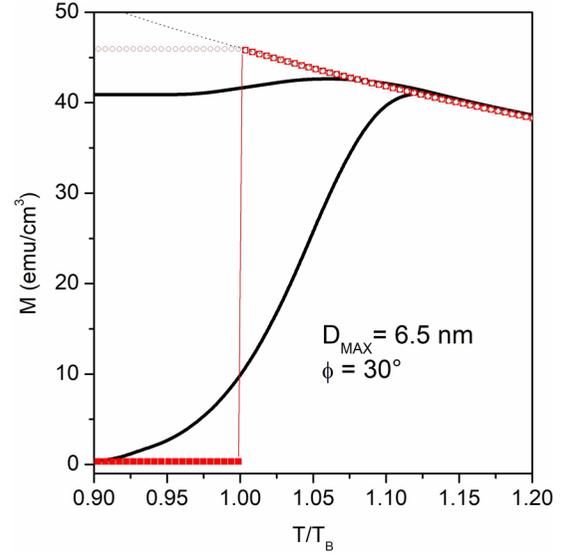
FIG. 5. Temperature behavior of FC and ZFC curves around T_B for monodisperse nanoparticles ($D = 6.5$ nm) with easy axis making the angle $\phi = 30°$ with respect to the field direction. Applied field $H = 10$ Oe. Black curves: exact solutions of rate equations with heating rate $\beta_h = 6$ K/min and cooling rate $\beta_c = 50$ K/min; full and dotted lines: linearized standard model based on Langevin-law properties [Eq. (12)]. Dotted line: equilibrium magnetization (exact solution).

and the exact solution obtained from the rate equations is given in Fig. 5 for the ZFC/FC curves of a monodisperse nanoparticle system.

(b) Above T_B, the expressions of Eq. (12) involve the linearization of the Langevin function.

For a DWS, the rate-equation model developed in the previous section can be linearized as well, using the same simplifying assumption as in (a), as discussed in Secs. III B and III C.

A. Linearized equilibrium magnetization curve

When the temperature is high enough that the parameter α (for a nanoparticle of given size and ϕ angle) can be written as $\alpha = \frac{E_2 - E_1}{k_B T} \simeq \frac{2M_s HV}{k_B T} \cos\phi \ll 1$, the overall equilibrium magnetization of a nanoparticle system becomes

$$M_{\text{eq}} = \frac{M_s^2 H}{2k_B T} \langle V \rangle + \frac{M_s^2 H}{4K_{\text{eff}}}, \quad (13)$$

where $\langle V \rangle$ is the average nanoparticle volume. This expression should be compared with the corresponding expression obtained from both lines of Eq. (12) at high temperature, i.e., $M_{\text{eq}}^{(L)} = \frac{M_s^2 H}{3k_B T} \langle V \rangle$. It should be explicitly noted that the second term of Eq. (13) is typically much smaller than the first one: Using the parameter values reported in Fig. 2 one finds that the first term dominates upon the second up to about 1000 K.

In the DWS model, the term in $1/T$ has a different numeric denominator, and an additional term is present. This is not unexpected, because even if at high temperature (such that $k_B T \gg E_2 - E_1$, so that $\alpha \approx 0$) the numbers N_1 and N_2
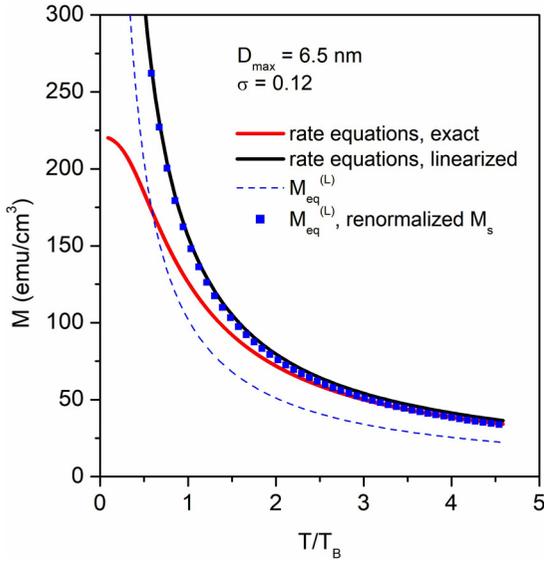
FIG. 6. Red line: reduced temperature dependence of the exact equilibrium magnetization obtained from the rate equations, for nanoparticles distributed according to a lognormal law (distribution parameters in the legend). Black line: linearization of the rate-equation model. Dashed line: standard model based on Langevin-law properties; in order to match this curve to the exact solution, M_s has to be renormalized by a factor $(3/2)^{1/2}$ so that the dashed curve is multiplied by a factor $3/2$ (blue dots).

become identical, the magnetization vectors $\vec{M}_1 = N_1\vec{\mu}$ and $\vec{M}_2 = N_2\vec{\mu}$ are still tilted away from the easy axis towards the direction of the field $\vec{H}$. Of course, such a persistent angle of tilt depends on the values of M_s and K_{eff}, which both decrease with increasing T. In any case, any further investigation of the high-temperature limit of the DWS model is useless, basically because at high temperatures (above $T \approx 5\langle T_B \rangle$) the description of nanoparticles as DWS loses validity and must be substituted by the usual superparamagnetic Langevin law [30].

An example of the exact equilibrium magnetization obtained by integrating the rate equations is given in Fig. 6 for nanoparticles distributed according to a lognormal law with average volume $\langle V \rangle$; this is compared with the linearized expression M_{eq}. The $M_{\text{eq}}^{(L)}$ curve is also reported; note that, when the second term in Eq. (13) is negligible, the saturation magnetization M_s in the expression for $M_{\text{eq}}^{(L)}$ must be rescaled by a factor $(3/2)^{1/2} \approx 1.22$ in order to match the exact equilibrium magnetization, as directly deduced from the expressions of M_{eq} and $M_{\text{eq}}^{(L)}$.

It should be explicitly noted that both linearized expressions of the equilibrium magnetization (i.e., M_{eq} and $M_{\text{eq}}^{(L)}$) have been developed in the hypothesis $\alpha \ll 1$. This is no longer a good approximation when the temperature is decreased, as clearly shown in Fig. 6. The deviation becomes non-negligible at $T \approx \langle T_B \rangle$ when the applied field magnitude is comparable to the ones used in typical measurements, and this brings about a wrong prediction of the behavior of the entire FC curve, as further discussed in Sec. III D. Strictly speaking, Eq. (13) is valid in the limit $H \to 0$ only.
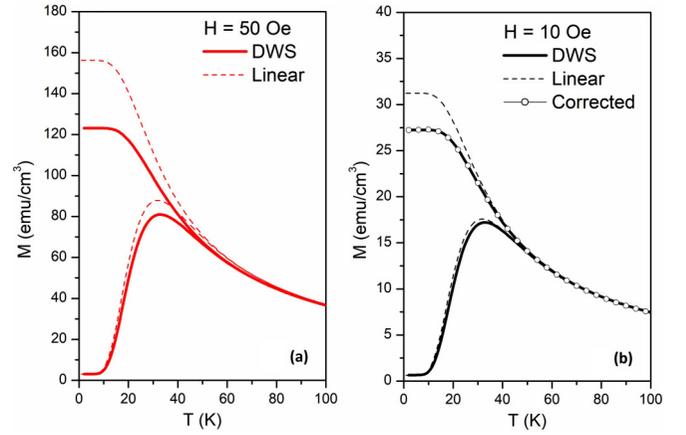
FIG. 7. Full lines: exact FC/ZFC curves for nanoparticles distributed according to a lognormal law ($D_{\text{max}} = 6.5$ nm, $\sigma = 0.12$). Physical parameters as in Fig. 2; heating rate $\beta_h = 6$ K/min, cooling rate $\beta_c = 50$ K/min. Dashed lines: FC/ZFC curves predicted by the linearized DWS model. Panel (a): $H = 50$ Oe; panel (b): $H = 10$ Oe. White circles in panel (b): corrected linear approximation of the FC curve (see text).

B. Linearized ZFC curve

The ZFC magnetization obtained by linearization of the rate equation (details in Appendix A 2) is

$$M_{\text{ZFC}} = \frac{M_s^2 H}{2k_B T} \int_0^{D_c(T)} V p(D) dD + \frac{M_s^2 H}{4K_{\text{eff}}} \quad (14)$$

which duly merges with the M_{eq} curve as $D_c \to \infty$.

C. Linearized FC curve, standard case

By "standard case" it is meant here that the maximum temperature T_{MAX} is well above the average blocking temperature $\langle T_B \rangle$. Usually this is an implicitly assumed condition, for instance in the second line of Eq. (12). However, as we shall see in Sec. V, in many experimental circumstances a different scheme needs to be introduced. The expression for the linearized FC curve (further details in Appendix A 3) is

$$\begin{aligned} M_{\text{FC}} &= \frac{M_s^2 H}{2k_B T} \int_0^{D_c(T)} V p(D) dD + \frac{M_s^2 H}{4K_{\text{eff}}} \\ &\quad + \frac{25 M_s^2 H}{2K_{\text{eff}}} \int_{D_c(T)}^{\infty} p(D) dD \\ &= M_{\text{ZFC}} + \frac{25 M_s^2 H}{2K_{\text{eff}}} \int_{D_c(T)}^{\infty} p(D) dD. \quad (15) \end{aligned}$$

Once again, M_{FC} merges with the M_{eq} curve (and with M_{ZFC}) as $D_c \to \infty$.

D. Range of validity of the linear approximations

Strictly speaking, all linear approximations are valid in the limit $H \to 0$. However, experimental data must be collected using a field sufficiently large to clearly detect the magnetic signal. Often a value in the range 10–100 Oe is used in both cooling and heating in order to minimize the noise to signal ratio. Figure 7 clearly shows that when $H = 50$ Oe (or

more) the linearized ZFC curve does not adequately match the exact curve; in particular it fails to reproduce the magnitude of the ZFC maximum; as a consequence, lower fields (e.g., $H = 10$–20 Oe) should be needed in real measurements in order to ensure that the linearized ZFC curve provides an accurate representation of the exact behavior of M_{ZFC}. This should be kept in mind while applying linearized expressions to analyze experimental ZFC curves obtained under fields larger than 20 Oe. Finally, it should be remarked that the linearized expression of Eq. (14), obtained starting from the DWS model which keeps its validity well above $\langle T_B \rangle$, has the remarkable advantage of better depicting experimental ZFC curves with respect to the available linearized formulas based on the Langevin-function scheme. On the other hand, the linearized FC curve turns out to be systematically higher than the exact FC curve, even at very low applied fields. This is explained by considering that the method for determining M_f^* in the linearized case involves the instantaneous freezing of the equilibrium magnetization of each nanoparticle as the decreasing temperature intersects T_B; as seen in Fig. 6, however, the linearized equilibrium magnetization fails to represent the exact equilibrium curve at T_B (in fact, it is systematically higher); consequently a wrong value of the frozen-in magnetization is predicted. This problem affects both the DWS model and the Langevin-law scheme. As a consequence, no linearized expression of the FC curve should be taken as reliable. As a matter of fact, it is possible to check that the exact FC curve $M_{FC}^{(R.E.)}$ can be obtained from the corresponding linearized expression M_{FC} [Eq. (15)] through a simple linear formula $M_{FC}^{(R.E.)} = M_{FC} - f(T)$ where $f(T)$ is an *ad-hoc* correction. For instance, in the case of Fig. 7 (right panel) the $M_{FC}^{(R.E.)}$ curve is very well approximated by taking the sigmoidal function $f(T) = A/[1 + (T/T_0)^p]$ with $A = 4.01$, $T_0 = 21.53$, $p = 4.46$. However, no general rule can be devised to relate the A, T_0, p parameters to the details of the $p(D)$ distribution (e.g., for a lognormal distribution, to D_{max}, σ) and to the amplitude of the applied field H.

IV. EXTRACTING THE P(D) DISTRIBUTION FROM THE ZFC CURVE

A. Evaluating the p(D) function for noninteracting nanoparticles

Valuable, if approximate information about the size distribution $p(D)$ of an assembly of nanoparticles is often extracted from FC/ZFC curves under somewhat restrictive conditions (noninteracting particles; constant values of M_s and K_{eff}). The standard method consists of getting the blocking-temperature distribution $p(T_B)$ first, from the derivative with respect to temperature of the difference $M_{FC} - M_{ZFC}$ [13,38,39]. The $p(V)$ or $p(D)$ distributions are then obtained in a straightforward way [39]. This method is implicitly based on the standard linearized expression for the FC/ZFC curves in the Langevin scheme [Eq. (12)]. However, we have shown in Sec. III C that the linearized expression definitely fails to approximate the real FC curve, making the outcome of this procedure rather uncertain.

Here a method is proposed, based on the linearized expression for noninteracting particles in the DWS scheme.

The advantage of the method is that it uses the ZFC curve only, which is well approximated at low applied fields by the linearized expression [Eq. (14)]. If M_s and K_{eff} are both constant, the (unnormalized) $p(D)$ function is:

$$p(D) = \frac{\pi}{k_B} \left(\frac{K_{eff}}{25} \right)^2 D^2 F(D) = const. \times D^2 F(D), \quad (16)$$

where:

$$F(D) = \frac{1}{M_s^2 H} \left\{ M'_{ZFC}(T(D)) + \frac{1}{T(D)} \left[M_{ZFC}(T(D)) - \frac{M_s^2 H}{4K_{eff}} \right] \right\}, \quad (17)$$

M'_{ZFC} being the derivative of the experimental $M_{ZFC}(T)$ curve with respect to temperature. The correspondence between T and D, derived by the standard expression between blocking temperature and volume, is:

$$T(D) = \frac{\pi}{6} \frac{K_{eff}}{25 k_B} D^3, \quad (18)$$

where D is the diameter of the particles which become blocked at the temperature T. It should be remarked that $F(D)$ is largely known from experiment; the only two quantities which can be used as adjustable parameters are the constants M_s and K_{eff} entering the (small) term $\frac{M_s^2 H}{4K_{eff}}$. After proper normalization of $p(D)$, the probability of a particle having diameter between D and $D + dD$ is $p(D)dD$. The explicit derivation of the normalized $p(D)$ function can be found in Appendix A 4.

B. Application of the method to real nanoparticle systems

Usually, real magnetic nanosystems are characterized by the presence of magnetic interparticle interactions ranging from weak to strong, the labels indicating a ratio of r.m.s. interaction energy to single-particle anisotropy energy lower or larger than unity, respectively [19]. Strongly interacting systems are characterized, e.g., by low-temperature collective states (such as the super-spin-glass state) having peculiar static/dynamical properties and off-equilibrium dynamics [19]. On the other hand, the behavior of weakly interacting systems may be described in terms of deviations from the ideal noninteracting superparamagnetic behavior. In this case, a way to account for the observed effects consists of substituting the single-particle anisotropy constant with an effective anisotropy constant K_{eff} [21] which approximately takes into account the effect of weak interactions, transforming a multibody problem into a single-particle problem.

As a consequence, the present model can be applied not only to truly noninteracting particle assemblies but also to systems of weakly interacting particles and can therefore be used to study specific materials fulfilling this condition. The ubiquitous nature of FC/ZFC curves in the specialized literature of magnetic nanoparticles makes the model intrinsically interesting because its results can be exploited, to some extent, even in the case of systems containing weakly interacting particles. The model's features and outcomes have been tested in three specific systems where the interactions are
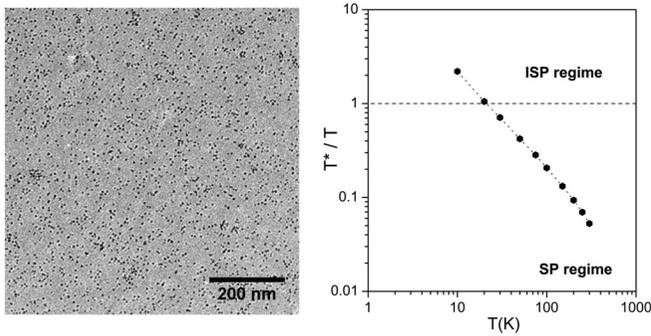
FIG. 8. Left panel: TEM image of magnetite particles dispersed in a polymer matrix; right panel: temperature behavior of the T^*/T ratio for the same material; T^* is a fictive interaction temperature in the ISP model.

so small that a single-particle picture (with an appropriate effective anisotropy) can be applied with some confidence.

The experimental ZFC curve of a dilute polymer-magnetite nanocomposite taken with an applied field $H = 25$ Oe is shown in Fig. 9(a). In this material the nanoparticles, having sizes in the range 4–8 nm with a Gaussian rather than log-normal distribution [40], are quite homogeneously distributed in the polymeric matrix with a mean interparticle distance of about 25 nm [see Fig. 8(a)]; the preparation process ensures that the nanoparticle axes are randomly distributed in the polymer matrix. The image clearly shows the absence of any significant contact interaction. The mean interparticle distance is so large that dipolar interparticle interactions can be safely considered as negligible (the r.m.s. dipolar energy being in this case as small as $\langle E_i^2 \rangle^{1/2} \sim 10 \times \mu^2/r^3 \sim 5 \times 10^{-16}$ erg) [41]. This conclusion is supported by the value of the T^*/T ratio [39], where T is the measurement temperature and T^* is a fictive interaction temperature introduced in the ISP (interacting superparamagnetism) model [42]. The temperature behavior of the T^*/T ratio is shown in Fig. 8(b). When the T^*/T ratio is less than unity, the system is in the superparamagnetic regime (interactions playing virtually no role on the magnetic properties); when this ratio is in the range 1–10, dipolar interactions, although no longer totally negligible, play a marginal role only [42]. In the present case, the T^*/T value never exceeds 2 at $T = 10$ K, becoming smaller than 1 before the maximum of the ZFC curve. As a consequence, the considered nanocomposite material can be viewed as an almost ideal system of basically noninteracting particles of known composition and shape [40] and is a most natural test ground for a practical assessment of the DWS model in its linearized form.

The experimental ZFC curve of a dilute polymer-magnetite nanocomposite taken with an applied field $H = 25$ Oe is shown in Fig. 9(a). Magnetic data [39] and TEM images [40] reveal that the nanoparticles, homogeneously distributed in the polymeric matrix, have sizes in the range 4–8 nm with a Gaussian rather than lognormal distribution [40]; the mean interparticle distance in the nanocomposite (about 25 nm, as deduced from TEM images [40]) is so large that dipolar interparticle interactions are completely negligible (the r.m.s. dipolar energy being in this case as small as $\langle E_i^2 \rangle^{1/2} \sim 10 \times$

$\mu^2/r^3 \sim 5 \times 10^{-16}$ erg) [41]. Therefore this material can be viewed as containing basically noninteracting, individual nanoparticles of known composition and shape [40] and is a most natural test ground for a practical assessment of the DWS model in its linearized form.

Figure 9(b) (full dots) shows the $p(D)$ curve obtained from Eq. (16) with $|K_{\text{eff}}| = 2.0 \times 10^5$ erg/cm^3 and $M_s = 350$ emu/cm^3. The latter value is fully consistent with the reduction of M_s usually observed in nanoparticles of similar composition [39,43–46]. Experimental values of the effective anisotropy constant in the range 1–3×10^5 erg/cm^3, obtained through a variety of techniques, are commonly reported in the literature for magnetite nanoparticles [47–51]. The experimental $p(D)$ curve turns out to be fully compatible with a Gaussian [red line in Fig. 9(a)] centered at $\langle D \rangle = 5.62$ nm, in excellent agreement with the value obtained by TEM image analysis (5.65 nm) [40]. The theoretical M_{ZFC} curve generated through Eq. (14) using the Gaussian $p(D)$ with the parameters reported in Fig. 9(b) is also displayed [green full line in 9(a)]. Even in this case, the agreement between model and experiment is remarkable up to about 35 K, i.e., above the temperature where the ZFC curve merges with the equilibrium curve of the DWS model [green dashed line in Fig. 9(a)]. At higher temperatures, the theoretical curve deviates from the experimental results, indicating that well above T_B the DWS scheme is no longer able to precisely describe the effect, as expected [30].

The experimental ZFC curves of two systems containing Ni subnanostructures (sample Ni 1) and lamellar sub-nanoparticles (sample Ni 2) decorating the surface of SiO$_2$ nanospheres are shown in Fig. 9(c). These ultrasmall magnetic units have been structurally and magnetically characterized in some detail [32]; in both cases, they can be considered as noninteracting and characterized by well-defined energy barriers, making it possible to describe them as DWS [32]. The Ni subnanostructures of sample Ni 1 are loosely distributed on the surface of nanospheres (diameter: 50 nm) and carry magnetic moments of the order of 100 μ_B; the dipolar interaction between any two subnanostructures is exceedingly small. Similar considerations hold for sample Ni 2 also. The symmetry axes of subnanostructures/subnanoparticles are randomly oriented [32].

Owing to the very weak magnetic signal, the experimental ZFC curves were taken with an applied field $H = 50$ Oe. Figure 9(d) shows the $p(D)$ curves obtained from Eq. (16) using anisotropy and magnetization values taken from the paper by Allia *et al.* [32] (full symbols). The experimental $p(D)$ curves of samples Ni 1 and Ni 2 can be fitted by two narrow Gaussians centered at 1.8 and 4.5 nm, respectively, in remarkably good agreement with TEM image analysis [32]. A tail of $p(D)$ towards the small size region can be observed in sample Ni 2.

V. ZFC AND FC CURVES HAVING A COMMON VERTEX AT ROOM TEMPERATURE

In a number of cases the FC/ZFC curves do not display the typical features of the ideal curves [typically, no peak of the ZFC curve is measured; no merging between FC and ZFC curves is observed; no common reversible (equilibrium)
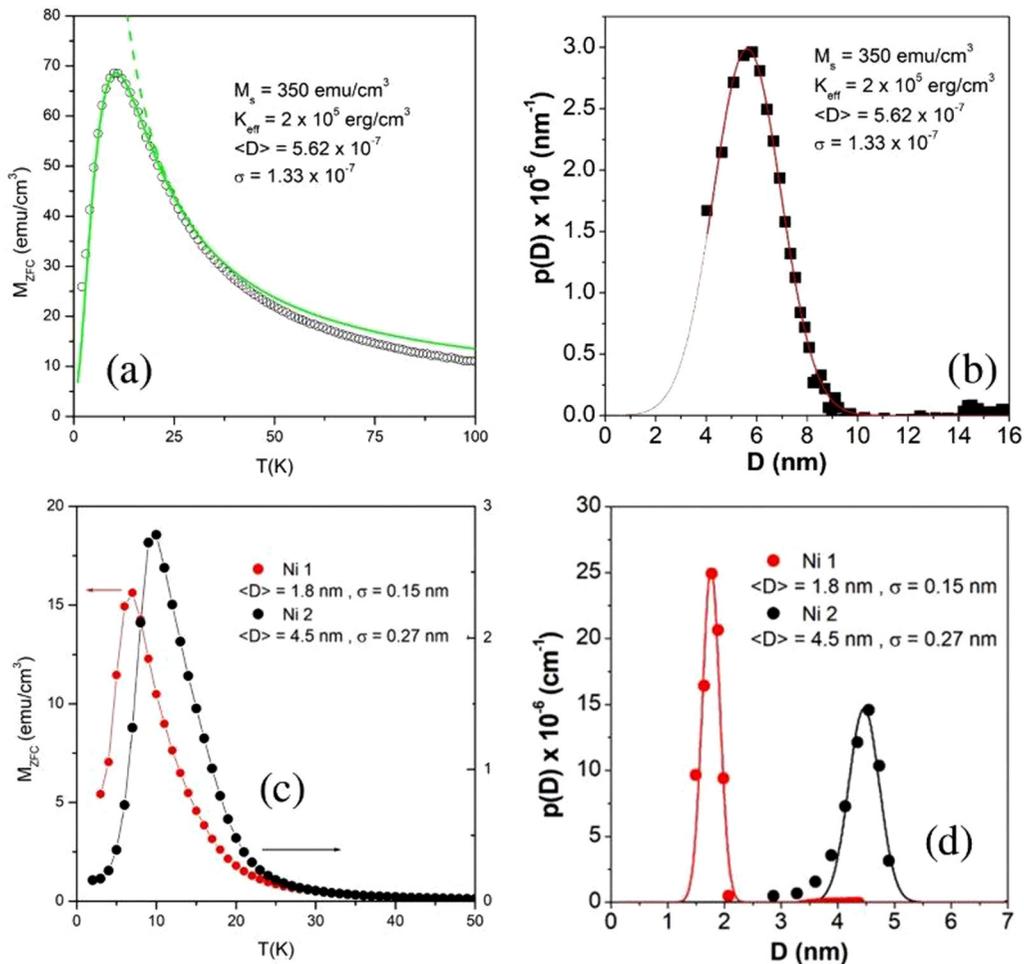
FIG. 9. (a) Symbols: experimental ZFC curve ($H = 25$ Oe) in a polymer-magnetite nanocomposite (material's details in the text); full green line: linearized model [DWS model, Gaussian $p(D)$]; dashed green line: equilibrium magnetization curve. (b) Symbols: corresponding size distribution function obtained applying the model to the experimental ZFC curve; red line: fitting Gaussian function. (c) Symbols: experimental ZFC curves ($H = 50$ Oe) in two systems containing Ni-rich subnanostructures (details in the text). (d) Symbols: corresponding size distribution functions obtained applying the model to the experimental ZFC curves; lines: fitting Gaussian functions.

region of M(T) can be identified]. Often both curves appear as almost featureless [43,52–57]. In these cases, the only common point of the two curves is at T_{MAX} (typically coincident with room temperature in the experimental practice); the two curves are well separated at every temperature below the common vertex at T_{MAX}. All such features can be understood in terms of the standard DWS model (i.e., without introducing explanations based on nanoparticle interactions) by explicitly taking into account that in these cases the average blocking temperature $\langle T_B \rangle$ of the system is well above T_{MAX}. The rate-equation model is able to produce correct FC/ZFC curves in this case also; however, it is preferable to study the linearized model first, in order to learn how to identify the relevant parameters playing a role in this important but poorly investigated case.

We explicitly consider the case of a set of noninteracting nanoparticles with sizes distributed according to the $p(D)$ law, such that $T_{\text{MAX}} < \langle T_B \rangle$. The ZFC curve is not modified by this condition and is still given by Eq. (13). Its final and

highest value is

$$M_{\text{ZFC}}(T_{\text{MAX}}) = \frac{M_s^2 H}{2 k_B T} \int_0^{D_{\text{MAX}}} V p(D) dD + \frac{M_s^2 H}{4 K_{\text{eff}}}, \quad (19)$$

where $D_{\text{MAX}} = \frac{6}{\pi} (25 k_B T_{\text{max}} / K_{\text{eff}})^{\frac{1}{3}}$. On the contrary, the expression of the FC curve changes substantially. First, the frozen-in value M_f^* depends on nanoparticle size (for simplicity here H_f is considered equal to H, so $M_f^* = M^*$):

(i) in nanoparticles with $D < D_{\text{MAX}}$, it is the equilibrium magnetization which freezes, exactly as in case (c) of Sec. 3, so that $M_{D<D_{\text{MAX}}}^* = (51/4)(M_s^2 H / K_{\text{eff}})$ (see Appendix A.2)

(ii) however, in nanoparticles with $D > D_{\text{MAX}}$ the blocking temperature T_B is larger than T_{MAX}: These particles are still blocked at T_{MAX} and their contribution to the frozen-in magnetization can be assumed to be $M_{D>D_{\text{MAX}}}^* = (1/4)(M_s^2 H / K_{\text{eff}})$, i.e., it is considerably lower than the previous value. This result and the underlying assumptions are discussed in Appendix A.5. The total frozen-in magnetization
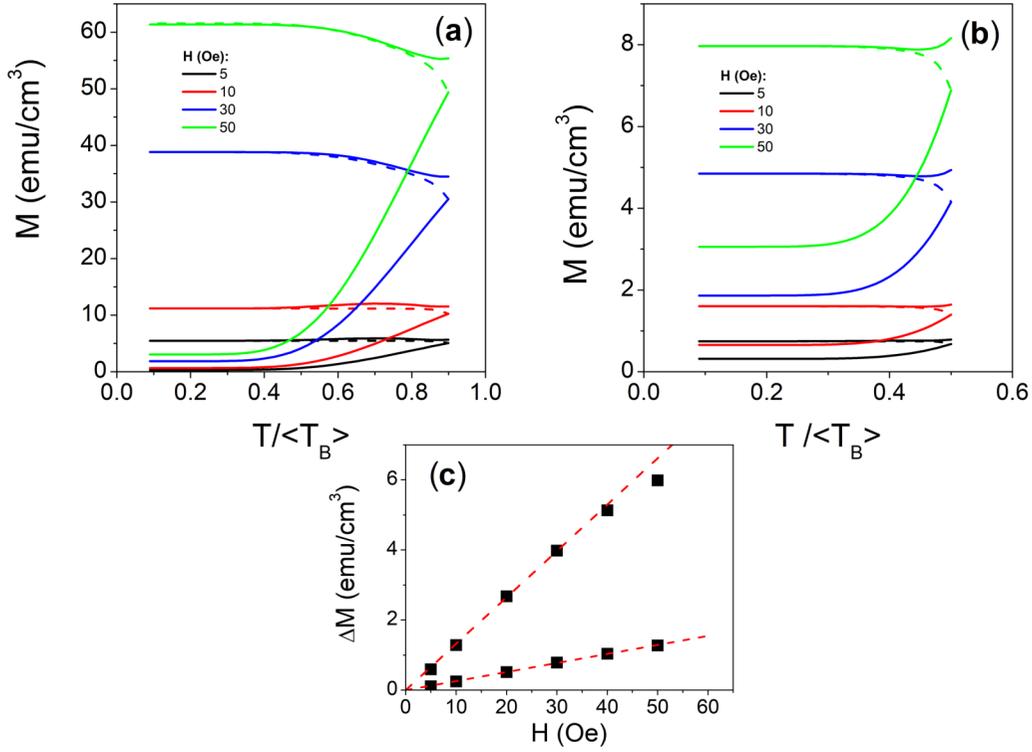
FIG. 10. Exact FC/ZFC curves for nanoparticles distributed according to a lognormal law ($D_{max} = 6.5$ nm, $\sigma = 0.12$) in the case $T_{MAX} < \langle T_B \rangle$. Physical parameters as in Fig. 2; heating rate $\beta_h = 6$ K/min, cooling rate $\beta_c = 6$ K/min. (a) $T_{MAX} = 0.90 \langle T_B \rangle$, (b) $T_{MAX} = 0.50 \langle T_B \rangle$. Full lines: FC/ZFC curves; dashed lines: cooling curves. Panel (c): FC-ZFC curve gap at T_{MAX}, $\Delta M(T_{MAX})$, as a function of H.

is therefore:

$$M^* = \frac{51}{4} \frac{M_s^2 H}{K_{eff}} \int_0^{D_{MAX}} p(D) dD + \frac{1}{4} \frac{M_s^2 H}{K_{eff}} \int_{D_{MAX}}^\infty p(D) dD$$
$$= \frac{25}{2} \frac{M_s^2 H}{K_{eff}} \int_0^{D_{MAX}} p(D) dD + \frac{1}{4} \frac{M_s^2 H}{K_{eff}}. \quad (20)$$

When T_{MAX} is very large and higher than $\langle T_B \rangle$ the expression reduces to $M^* = (51/4)(M_s^2 H/K_{eff})$ as in case (c) of Sec. 3.

In the calculation of the M_{FC} curve starting from the M^* value determined by Eq. (20), the contribute of nanoparticles with $D < D_{MAX}$ must be considered separately from the one of nanoparticles with $D > D_{MAX}$:

(i) for nanoparticles with $D < D_{MAX}$ ($T_B < T_{MAX}$) two temperature regions must be considered:

(ii) $0 \leqslant T \leqslant T_B$: blocked state, and $dM_{FC}^{(1)} = (51/4)(M_s^2 H/K_{eff}) p(D) dD$;

(iii) $T_B \leqslant T \leqslant T_{MAX}$: equilibrium state, and $dM_{FC}^{(2)} = \{(M_s^2 H V)/(2k_B T) + (1/4)(M_s^2 H/K_{eff})\} p(D) dD$;

(iv) on the contrary, the nanoparticles with $D > D_{MAX}$ ($T_B > T_{MAX}$) remain in the blocked state over the entire interval, so that $dM_{FC}^{(3)} = (1/4)(M_s^2 H/K_{eff}) p(D) dD$. The overall FC magnetization curve is therefore expressed as the sum of the three independent contributions comprehensive of all

nanoparticle sizes:

$$M_{FC} = \frac{51}{4} \frac{M_s^2 H}{K_{eff}} \int_{D_c(T)}^{D_{MAX}} p(D) dD$$
$$+ \frac{M_s^2 H}{2k_B T} \int_0^{D_c(T)} V p(D) dD$$
$$+ \frac{1}{4} \frac{M_s^2 H}{K_{eff}} \int_0^{D_c(T)} p(D) dD$$
$$+ \frac{1}{4} \frac{M_s^2 H}{K_{eff}} \int_{D_{MAX}}^\infty p(D) dD. \quad (21)$$

This expression can be easily rewritten as:

$$M_{FC} = \frac{M_s^2 H}{2k_B T} \int_0^{D_c(T)} V p(D) dD + \frac{1}{4} \frac{M_s^2 H}{K_{eff}}$$
$$+ \frac{25}{2} \frac{M_s^2 H}{K_{eff}} \int_{D_c(T)}^{D_{MAX}} p(D) dD$$
$$= M_{ZFC} + \frac{25}{2} \frac{M_s^2 H}{K_{eff}} \int_{D_c(T)}^{D_{MAX}} p(D) dD. \quad (22)$$

It is immediately checked from Eq. (22) that when $T = T_{MAX}$, $D_c(T) = D_{MAX}$, so that $M_{FC} = M_{ZFC}$ (vertex point). This equality does not mean that at T_{MAX} the system is at equilibrium, though. When T_{MAX} is very large Eq. (22)
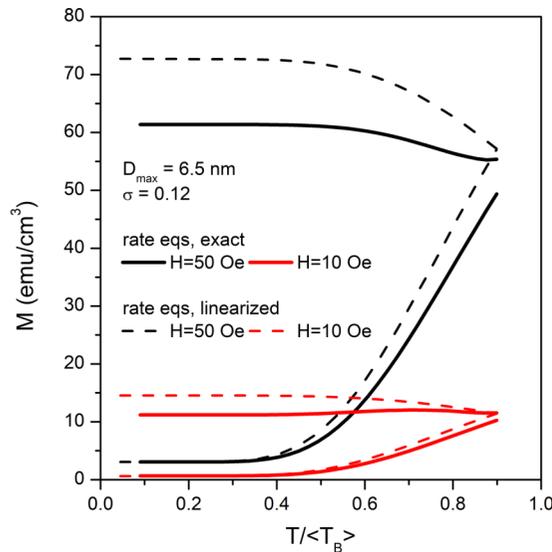
FIG. 11. Comparison between exact (full lines) and linearized (dashed lines) FC/ZFC curves for nanoparticles distributed according to a lognormal law ($D_{max} = 6.5$ nm, $\sigma = 0.12$) in the case $T_{MAX} = 0.90\langle T_B \rangle$. Physical parameters as in Fig. 2; $H = 50$ Oe; heating rate $\beta_h = 6$ K/min, cooling rate $\beta_c = 6$ K/min.

reduces to Eq. (15); actually, when T_{MAX} is much higher than $\langle T_B \rangle$, M_{FC} merges with M_{ZFC} at equilibrium.

As anticipated, the rate-equation model provides exact solutions even in the case $T_{MAX} < \langle T_B \rangle$. An example is given in Figs. 10(a) and 10(b) where the exact ZFC and FC curves have been calculated in the cases $T_{MAX} = 0.9\langle T_B \rangle$ and $T_{MAX} = 0.5\langle T_B \rangle$ with a field H in the range 5–50 Oe. In this case, the cooling rate β_c was taken equal to 6 K/min instead of 50 K/min in order to better represent the actual experimental conditions (in fact, the maximum measurement temperature cannot exceed T_B which is equal to 22 K for the considered system [Fig. 7(a)]); such a low rate is needed in order to maintain a controlled cooling of the sample in this narrow temperature region. The behavior of the magnetization on cooling under the same field H is also shown (dashed lines). It should be remarked that the shape of the FC curve is critically dependent on the distance of T_{MAX} from $\langle T_B \rangle$; in particular, the FC curve can monotonically decrease with increasing temperature, as in Fig. 10(a), or show a change in slope as in Fig. 10(b). These features are generally explained by considering that both FC and ZFC curves reflect the tendency of unblocking particles to reach the equilibrium state, which is characterized by a much higher magnetization value.

Exact and linearized expressions are compared in Fig. 11; in the case $T_{MAX} = 0.9\langle T_B \rangle$ with $H = 50$ Oe and the cooling rate β_c was taken equal to 6 K/min. Figures 10 and 11 clearly show that the exact curves become indeed close to each other at the vertex, but they are not coincident as the linearized model predicts; in particular, the rate equations bring the ending point of the exact FC curve above the one of the exact ZFC curve. The difference is $\Delta M = M_{FC}(T_{MAX}) - M_{ZFC}(T_{MAX})$ which decreases with reducing H and disappears for $H \rightarrow 0$, as shown in Fig. 10(c). This confirms that the linearized model predictions becomes exact for $H \rightarrow 0$. If the measurement

field is not small enough, the experimental curves are expected not to meet at T_{MAX}, as actually sometimes reported [52,55,57]. Despite the limitations of the linearized model for any finite H value, Eq. (22) appears as an expedient expression to study FC/ZFC curves in the case of curves having a common vertex at room temperature.

VI. CONCLUSIONS

The rate-equation model in the DWS scheme appears as able to depict the behavior of low-field magnetization of a system of non-/weakly interacting nanoparticles submitted to the FC/ZFC measurement procedure. The solving method requires simple calculation tools and limited machine time. Describing the nanoparticle behavior in terms of a DWS system even above the blocking temperature has been shown to be not only possible but preferable, at least for a maximum temperature of investigation not larger than about $5\langle T_B \rangle$. The rate-equation method allows one not only to obtain the magnetization curves in both ZFC and FC conditions but also to follow and exactly evaluate the freezing of magnetization on cooling; as a result, the initial value of the ensuing FC curve is described much more accurately than by the linearized expression, which fails to predict both magnitude and shape and of a real FC curve.

Linearization of the rate-equation model leads to explicit expressions for both ZFC and FC curves having non-negligible differences from the similar formulas existing in the literature; it has been shown that the intrinsic magnetization of nanoparticles (hence the magnetic moment on each nanoparticle) is systematically overestimated by fitting the ZFC curve with an expression based on linearization of the Langevin function.

A method to determine the size distribution of polydisperse nanoparticles has been derived starting from the linearized expression of the ZFC curve in the DWS scheme. This procedure has the advantage over the existing methods of avoiding all drawbacks related to the failure of the linearized expression to correctly represent the real FC curve.

Finally, the model has been applied to the case of a blocking temperature larger than the maximum investigated temperature (usually equal to room temperature). In this case, a different linearized expression has been put forward, whose structure accounts for the existence and the characteristic shape of FC/ZFC curves having in common a single vertex at T_{MAX}.

The DWS model and its linearization are based upon a noninteracting particle picture; therefore, the results of the present study cannot be applied to strongly interacting nanoparticle systems where different blocking/unblocking mechanisms and a different approach to equilibrium are expected. On the other hand a reasonably accurate, if approximate, picture of *weakly* interacting systems can be obtained by using a description in terms of noninteracting particles as a starting point and subsequently turning the interaction on. As a consequence, the present model is deemed able to provide first-hand information about the real $p(D)$ curve of weakly interacting nanoparticles using purely magnetic data. This result can be in turn compared to the one obtained from structural/morphological characterization (e.g., TEM image analysis) allowing one to

extract accurate information about ill-known physical quantities such as the (effective) anisotropy constant. Compared to other existing approaches, the present model has the notable advantage of estimating the size distribution of nanoparticles by making use of a single experimental curve (ZFC) instead of the difference between two curves (FC and ZFC), therefore markedly reducing the uncertainty involved in the numerical treatment of data. Finally, the model shows that the cooling rate has non-negligible effects on the subsequent measurements and particularly on the value and shape of the FC curve; usually this fact is not properly taken into account in the existing approaches and can be exploited in specific measurements to investigate the actual dynamics of particle blocking.

APPENDIX

1. Approximate value of M_f^* for small tilt angles

When $H \to 0$ so that both angles of tilt away from the easy-axis directions 0, π, are very small, the angular terms in Eq. (4) can be transformed:

$$\cos(\theta_1 - \phi) = \cos(\epsilon_1 - \phi) \simeq \cos\phi + \epsilon_1\sin\phi,$$
$$\cos(\theta_2 - \phi) = \cos(\pi - \epsilon_2 - \phi) \simeq -\cos\phi + \epsilon_2\sin\phi.$$

The two small angles of tilt are found by minimizing Eq. (3) for small tilt; ϵ_1 and ϵ_2 are equal in this limit:

$$\epsilon_1 = \epsilon_2 = \epsilon = \frac{M_s H \sin\phi}{2K_{\text{eff}} + M_s H \cos\phi} \simeq \frac{M_s H}{2K_{\text{eff}}}\sin\phi. \quad \text{(A1)}$$

Starting from Eq. (8), the magnetization frozen at $T_{\min}$ becomes:

$$M_f^* = M_1(T_{\min})[\cos\phi + \epsilon\sin\phi + \cos\phi - \epsilon\sin\phi]$$
$$- M_{s\phi}\cos\phi + \epsilon M_{s\phi}\sin\phi,$$
$$= [2M_1(T_{\min}) - M_{s\phi}]\cos\phi + \epsilon Ms\phi\sin\phi.$$

Making use of Eq. (10) and Eq. (A1) one gets:

$$M_f^* = M_{\text{intr}}^* + \epsilon M_{s\phi}\sin\phi = M_{\text{intr}}^* + M_{s\phi}\frac{M_s H}{2K_{\text{eff}}}\sin^2\phi,$$

as reported in the text.

2. Linearized zfc curve

The blocking temperature defines two distinct temperature regions:

(i) when $T < T_B$, $M_1 = M_{s\phi}/2$. Taking into account Eq. (4) and Eq. (A1), the magnetization of nanoparticles of size D under a magnetic field applied at the angle ϕ is:

$$M_{\text{ZFC}} = \frac{M_{s\phi}}{2}2\cos\phi - M_{s\phi}\cos\phi + \epsilon M_{s\phi}\sin\phi$$
$$= M_{s\phi}\frac{M_s H}{2K_{\text{eff}}}\sin^2\phi$$

which results in $M_{\text{ZFC}} = (M_s^2 H)/(4K_{\text{eff}})$ after summing over all angles;

(ii) when $T > T_B$,

$$M_{\text{ZFC}} = M_{\text{eq}} = \frac{M_s^2 HV}{2k_B T} + \frac{M_s^2 H}{4K_{\text{eff}}}$$

according to Eq. (13). Note that M_{ZFC} is discontinuous at T_B. Summing over all sizes distributed according to the $p(D)$ law results in:

$$M_{\text{ZFC}} = \frac{M_s^2 H}{2k_B T}\int_0^{D_c(T)} Vp(D)dD$$
$$+ \frac{M_s^2 H}{4K_{\text{eff}}}\left(\int_0^{D_c(T)} p(D)dD + \int_{D_c(T)}^{\infty} p(D)dD\right),$$

which is coincident with Eq. (14).

3. Linearized fc curve (standard case, $T_{\text{MAX}} \gg \langle T_B \rangle$)

For nanoparticles of size D under a magnetic field $H_f = H$ applied at the angle ϕ, the magnetization frozen on cooling is by definition:

$$M^* = M_{s\phi}\left(\frac{M_s HV}{k_B T_B}\cos^2\phi + \frac{M_s H}{2K_{\text{eff}}}\sin^2\phi\right).$$

Expressing T_B in terms of V one immediately gets:

$$M^* = M_{s\phi}\left(\frac{25M_s H}{K_{\text{eff}}}\cos^2\phi + \frac{M_s H}{2K_{\text{eff}}}\sin^2\phi\right).$$

Summing over all angles results in:

$$M^* = \frac{25M_s^2 H}{2K_{\text{eff}}} + \frac{M_s^2 H}{4K_{\text{eff}}} = \frac{51M_s^2 H}{4K_{\text{eff}}}.$$

Therefore, the magnetization measured during heating takes the following values:

(i) when $T < T_B$,

$$M_{\text{FC}} = M^* = \left(51M_s^2 H\right)/(4K_{\text{eff}})$$

(ii) when $T > T_B$,

$$M_{\text{FC}} = M_{\text{eq}} = \frac{M_s^2 HV}{2k_B T} + \frac{M_s^2 H}{4K_{\text{eff}}}$$

according to Eq. (13). Note that M_{FC} is continuous at T_B. After summing over all sizes distributed according to the $p(D)$ law, one gets:

$$M_{\text{FC}} = \frac{M_s^2 H}{2k_B T}\int_0^{D_c(T)} Vp(D)dD + \frac{M_s^2 H}{4K_{\text{eff}}}\int_0^{D_c(T)} p(D)dD$$
$$+ \frac{51M_s^2 H}{4K_{\text{eff}}}\int_{D_c(T)}^{\infty} p(D)dD,$$

which is easily transformed into Eq. (15).

4. Derivation of the size distribution function

The derivative with respect to the temperature of the ZFC curve, as expressed by the linearized form of the DWS model

[Eq. (10)], is:

$$\frac{dM_{\text{ZFC}}}{dT} = -\frac{M_s^2 H}{2k_B T^2} \int_0^{D(T)} V' p(D') dD'$$
$$+ \frac{M_s^2 H}{2k_B T} \frac{\pi}{6} \frac{d}{dD} \int_0^{D(T)} D'^3 p(D') dD' \times \frac{dD}{dT},$$

where $D(T)$ is the diameter of particles which undergo blocking at the temperature T [see Eq. (14)]. Using

$$D = \left(\frac{6}{\pi} \frac{25 k_B}{K_{\text{eff}}}\right)^{\frac{1}{3}} T^{\frac{1}{3}} \equiv \delta T^{\frac{1}{3}} \qquad (A2)$$

one gets:

$$\frac{dD}{dT} = \frac{1}{3} \delta T^{-\frac{2}{3}} = \frac{\delta^3}{3D^2}.$$

Taking into account the definition of M_{ZFC} [Eq. (14)] it is possible to write:

$$\frac{dM_{\text{ZFC}}}{dT} = -\frac{1}{T}\left(M_{\text{ZFC}}(T) - \frac{M_s^2 H}{4K_{\text{eff}}}\right)$$
$$+ \frac{M_s^2 H}{2k_B T} \frac{\pi}{6} D^3 p(D) \frac{\delta^3}{3D^2}.$$

Transforming the $1/T$ factor in the last term by means of Eq. (18) and rearranging one gets:

$$\frac{dM_{\text{ZFC}}}{dT} + \frac{1}{T(D)}\left(M_{\text{ZFC}}(T(D)) - \frac{M_s^2 H}{4K_{\text{eff}}}\right)$$
$$= \frac{M_s^2 H}{2k_B} \frac{\delta^3}{D^3} \frac{\pi}{6} D^3 p(D) \frac{\delta^3}{3D^2}.$$

Calling $M_s^2 H F(D)$ the left-side term and taking into account Eq. (A2), the latter expression easily transforms into:

$$\frac{M_s^2 H}{2k_B} \frac{\pi}{6} p(D) \frac{\delta^6}{3D^2} = \frac{25^2 M_s^2 H k_B}{\pi K_{\text{eff}}^2} \frac{p(D)}{D^2} = M_s^2 H F(D)$$

or

$$p(D) = \frac{\pi K_{\text{eff}}^2}{25^2 k_B} D^2 F(D).$$

With the present assumptions, the multiplying factor of the above expression is a constant. The $F(D)$ function rapidly goes to zero (faster than $1/D^6$) as D increases, so that the integral $\int_0^\infty D^2 F(D) dD$ is equal to some finite value A which

can be determined by numerical integration of the experimental data. The normalized occurrence frequency $p(D)dD$ is therefore

$$p(D)dD = \frac{1}{A} D^2 F(D) dD.$$

5. Frozen-in magnetization of particles which are still blocked at T_{MAX}

If T_{MAX} is lower than the average blocking temperature $\langle T_B \rangle$ of a set of nanoparticles distributed in size, a substantial fraction of particles are and remain blocked over the entire range of investigated temperatures, $T_{\text{min}} \leqslant T \leqslant T_{\text{MAX}}$. As previously clarified, the contribution to the total frozen-in magnetization M_f^* on cooling from T_{MAX} under the field $H_f = H$ can be thought of as the sum of an intrinsic contribution M_{intr}^* related to the uneven distribution of DWS in the two wells by effect of the cooling field H_f and of a second contribution related to the angles of tilt θ_{1f}, θ_{2f} away from the $0,\pi$ directions in each well. Making use of Eq. (9), the latter term (when summed over all angles ϕ) is:

$$M_f^* - M_{\text{intr}}^* = \frac{M_s^2 H}{4K_{\text{eff}}}.$$

The question arises how large the intrinsic contribution M_{intr}^* is in the case of nanoparticles still blocked at T_{MAX}. Clearly the small field H_f is not enough to modify the distribution of these DWS in the two wells: Such a distribution should be considered as fully blocked. In principle, a nonzero M_{intr}^* should arise from any uneven distribution of the considered DWS in the two wells generated in the previous magnetothermal history of the material: Such an uneven distribution would be stable, i.e., not destroyed by thermal disorder if the sample is kept at T_{MAX} (usually corresponding to room temperature). However, it is possible to safely assume that the distribution of these DWS in the two wells is even. The standard procedure of FC/ZFC curve measurements requires that the sample be accurately demagnetized (e.g., under a strong alternating field whose amplitude is gradually reduced with time) before starting the measurement cycle proper. As a consequence, the two wells of the considered DWS can be thought of as being evenly populated, the equally distributed population being obtained by the action of the demagnetizing field rather than the one of temperature. Even if these two effects are intrinsically different in nature, one can conclude that $M_{\text{intr}} \approx 0$ for all nanoparticles having blocking temperature higher than T_{MAX}. Therefore $M_{D>D_{\text{MAX}}}^* = \frac{1}{4}(M_s^2 H / 4K_{\text{eff}})$ as used in Sec. 5.

[1] D. Lisjak and A. Mertelj, Prog. Mater. Sci. **95**, 286 (2018).

[2] P. Kumar, K.-H. Kim, V. Bansal, T. Lazarides, and N. Kumar, J. Ind. Eng. Chem. **54**, 30 (2017).

[3] S.-H. Hung and K. McKenna, Phys. Rev. Mater. **1**, 024405 (2017).

[4] L. Mohammed, H. G. Gomaa, D. Ragab, and J. Zhu, Particuology **30**, 1 (2017).

[5] I. Goychuk, Phys. Rev. E **92**, 042711 (2015).

[6] K. K. Kefeni, B. B. Mamba, and T. A. M. Msagati, Sep. Purif. Technol. **188**, 399 (2017).

[7] M.-K. Kim, J. Sim, J.-H. Lee, M. Kim, and S.-K. Kim, Phys. Rev. Appl. **9**, 054037 (2018).

[8] M. Angelakeris, Biochim. Biophys. Acta **1861**, 1642 (2017).

[9] K. H. J. Buschow, *Handbook of Magnetic Materials* (Elsevier, Amsterdam, 2015), Vol. 23.

[10] O. Fruchart, *Lecture notes on Nanomagnetism* http://fruchart.eu/olivier/publications/index.html (2014).

[11] D. Peddis, P. E. Jonsson, S. Laureti, and G. Varvaro, in *Nanomagnetism: Fundamentals and Applications*, edited by C. Binns (Elsevier, Oxford, 2014), Vol. 6, Chap. 4, pp. 129–188.

[12] C. Papusoi Jr., Al. Stancu, and J. L. Dormann, J. Magn. Magn. Mater. **174**, 236 (1997).

[13] H. Mamiya, M. Ohnuma, I. Nakatani, and T. Furubayashim, IEEE Trans. Magn. **41**, 3395 (2005).

[14] M. Knobel, W. C. Nunes, L. M. Socolovsky, E. De Biasi, J. M. Vargas, and J. C. Denardin, J. Nanosci. Nanotechnol. **8**, 2836 (2008).

[15] M. F. Hansen and S. Mørup, J. Magn. Magn. Mater. **203**, 214 (1999).

[16] P. A. Joy, P. S. A. Kumar, and S. K. Date, J. Phys.: Condens. Matter **10**, 11049 (1998).

[17] J. García-Otero, M. Porto, J. Rivas, and A. Bunde, Phys. Rev. Lett. **84**, 167 (2000).

[18] C. Papusoi Jr., J. Magn. Magn. Mater. **195**, 708 (1999).

[19] D. Fiorani and D. Peddis, J. Phys.: Conf. Series **521**, 012006 (2014).

[20] R. W. Chantrell, M. El-Hilo, and K. O' Grady, IEEE Trans. Magn. **27**, 3570 (1991).

[21] S. Mørup and E. Tronc, Phys. Rev. Lett. **72**, 3278 (1994).

[22] J. M. Vargas, W. C. Nunes, L. M. Socolovsky, M. Knobel, and D. Zanchet, Phys. Rev. B **72**, 184428 (2005).

[23] F. H. Sanchez, P. Mendoza Zelis, M. L. Arciniegas, G. A. Pasquevich, and M. B. Fernandez van Raap, Phys. Rev. B **95**, 134421 (2017).

[24] N. A. Usov, J. Appl. Phys. **109**, 023913 (2011).

[25] S. Chakraverty, M. Bandyopadhyay, S. Chatterjee, S. Dattagupta, A. Frydman, S. Sengupta, and P. A. Sreeram, Phys. Rev. B **71**, 054401 (2005).

[26] M. Bandyopadhyay and S. Dattagupta, Phys. Rev. B **74**, 214410 (2006).

[27] M. Sasaki, P. E. Jönsson, H. Takayama, and H. Mamiya, Phys. Rev. B **71**, 104405 (2005).

[28] G. M. Tsoi, L. E. Wenger, U. Senaratne, R. J. Tackett, E. C. Buc, R. Naik, P. P. Vaishnava, and V. Naik, Phys. Rev. B **72**, 014445 (2005).

[29] A. P. Guimaraes, *Principles of Magnetism* (Springer, Heidelberg, 2009).

[30] O. Fruchart, P.-O. Jubert, C. Meyer, M. Klaua, J. Barthel, and J. Kirschner, J. Magn. Magn. Mater. **239**, 224 (2002).

[31] O. Fruchart and A. Thiaville, C. R. Phys. **6**, 921 (2005).

[32] G. Barrera, G. Alberto, P. Tiberto, G. Martra, and P. Allia, Sci. Rep. **7**, 10822 (2017).

[33] B. D. Cullity and C. D. Graham, *Introduction to Magnetic Materials*, 2nd ed. (IEEE Press, Wiley, Hoboken, 2009).

[34] J. M. D. Coey, *Magnetism and Magnetic Materials* (Cambridge University Press, Cambridge, 2009).

[35] C. H. Back, R. Allenspach, W. Weber, S. S. P. Parkin, D. Weller, E. L. Garwin, and H. C. Siegmann, Science **285**, 864 (1999).

[36] See Supplemental Material at http://link.aps.org/supplemental/10.1103/PhysRevB.98.134423 for details of the computational

procedure and an example of the effect of cooling rate on the frozen magnetization.

[37] D. Kechrakos, in *Handbook of Nanophysics: Nanoparticles and Quantum Dots*, edited by K. D. Sattler (CRC Press, Boca Raton, 2016).

[38] J. S. Micha, B. Dieny, J. R. Régnard, and J. F. Jacquot, J. Magn. Magn. Mater. **272–276**, e967 (2004).

[39] P. Allia, G. Barrera, P. Tiberto, T. Nardi, Y. Leterrier, and M. Sangermano, J. Appl. Phys. **116**, 113903 (2014).

[40] T. Nardi, M. Sangermano, Y. Leterrier, P. Allia, P. Tiberto, and J.-A. E. Manson, Polymer **54**, 4472 (2013).

[41] S. Mørup, Europhys. Lett. **28**, 671 (1994).

[42] P. Allia, M. Coisson, P. Tiberto, F. Vinai, M. Knobel, M. A. Novak, and W. C. Nunes, Phys. Rev. B **64**, 144420 (2001).

[43] D. Caruntu, G. Caruntu, and C. J. O' Connor, J. Phys. D: Appl. Phys. **40**, 5801 (2007).

[44] C. Sciancalepore, A. F. Gualtieri, P. Scardi, Albert Flor, P. Allia, P. Tiberto, G. Barrera, M. Messori, and F. Bondioli, Mater. Chem. Phys. **207**, 337 (2018).

[45] A. E. Berkowitz, W. J. Schuele, and P. J. Flanders, J. Appl. Phys. **39**, 1261 (1968).

[46] J. P. Chen, C. M. Sorensen, K. J. Klabunde, G. C. Hadjipanayis, E. Devlin, and A. Kostikas, Phys. Rev. B **54**, 9288 (1996).

[47] E. Lima Jr., A. L. Brandl, A. D. Arelaro, and G. F. Goya, J. Appl. Phys. **99**, 083908 (2006).

[48] P. Allia, P. Tiberto, M. Coisson, A. Chiolerio, F. Celegato, F. Vinai, M. Sangermano, L. Suber, and G. Marchegiani, J. Nanopart. Res. **13**, 5615 (2011).

[49] H. Nemala, J. S. Thakur, V. M. Naik, P. P. Vaishnava, G. Lawes, and R. Naik, J. Appl. Phys. **116**, 034309 (2014).

[50] C. Nayek, K. Manna, A. A. Imam, A. Y. Alqasrawi, and I. M. Obaidat, Conf. Series: Mater. Sci. Eng. **305**, 012012 (2018).

[51] V. N. Nikiforov, Yu. A. Koksharov, S. N. Polyakov, A. P. Malakho, A. V. Volkov, M. A. Moskvina, G. B. Khomutov, and V. Yu. Irkhin, J. Alloy Compd. **569**, 58 (2013).

[52] M. Uva, L. Mencuccini, A. Atrei, C. Innocenti, E. Fantechi, C. Sangregorio, M. Maglio, M. Fini, and R. Barbucci, Gels **1**, 24 (2015).

[53] G. Barrera, C. Sciancalepore, M. Messori, P. Allia, P. Tiberto, and F. Bondioli, Eur. Polym. J. **94**, 354 (2017).

[54] M. A. Peck, Y. Huh, R. Skomski, R. Zhang, P. Kharel, M. D. Allison, D. J. Sellmyer, and M. A. Langell, J. Appl. Phys. **109**, 07B518 (2011).

[55] M. A. Gonzalez-Fernandez, T. E. Torres, M. Andres-Verges, R. Costo, P. de la Presa, C. J. Serna, M. P. Morales, C. Marquina, M. R. Ibarra, and G. F. Goya, J. Solid State Chem. **182**, 2779 (2009).

[56] N. F. Huls, M-H. Phan, A. Kumar, S. Mohapatra, S. Mohapatra, P. Mukherjee, and H. Srikanth, Sensors **13**, 8490 (2013).

[57] M. Andrés-Vergés, R. Costo, A. G. Roca, J. F. Marco, G. F. Goya, C. J. Serna, and M. P. Morales, J. Phys. D: Appl. Phys. **41**, 134003 (2008).